

Identification of shallow Al donors in Al-doped ZnO nanocrystals: EPR and ENDOR spectroscopy

Serguei B. Orlinskii* and Jan Schmidt

Department of Physics, Huygens Laboratory, Leiden University, P.O. Box 9505, 2300 RA Leiden, The Netherlands

Pavel G. Baranov†

A. F. Ioffe Physico-Technical Institute, Russian Academy of Sciences, St. Petersburg 194021, Russia

Volker Lormann and Ingo Riedel

Functional Materials for Energy Technology, Bavarian Centre for Applied Energy Research (ZAE Bayern), Am Hubland, 97074 Würzburg, Germany

Daniel Rauh and Vladimir Dyakonov‡

Experimental Physics VI, Faculty of Physics and Astronomy, University of Würzburg, Am Hubland, 97074 Würzburg, Germany

(Received 9 August 2007; published 18 March 2008)

Electron paramagnetic resonance and electron-nuclear double resonance (ENDOR) experiments on ZnO nanoparticles doped with Al reveal the presence of shallow, effective-masslike donors related to substitutional Al atoms. The shallow character of the Al donor is evidenced by the multitude of ENDOR transitions of the ^{67}Zn nuclear spins and by the hyperfine interaction of 1.45 MHz of the ^{27}Al nuclear spin, which is much smaller than for atomic aluminum. The electric-field gradients at the Al and Zn atoms are found to be nearly the same, which supports the contention that the Al atom is located at a Zn position.

DOI: [10.1103/PhysRevB.77.115334](https://doi.org/10.1103/PhysRevB.77.115334)

PACS number(s): 73.22.-f, 76.30.Da, 61.72.uj, 76.70.Dx

I. INTRODUCTION

ZnO is a direct wide-band-gap semiconductor (energy gap of 3.35 eV at room temperature) and crystallizes in the wurtzite structure. Since it is a strong emitter, it attracts considerable attention for applications as ultraviolet (UV) light-emitting diodes and laser diodes.¹ The attractiveness of ZnO nanocrystals is that the confinement of the electronic wave function allows the tuning of the optical and electronic properties. The high free-exciton binding energy of 60 meV implies that the excitons are stable at room temperature. This binding energy increases further in confined systems and the luminescence efficiency of ZnO nanocrystals can be much higher than that of bulk ZnO crystals. Doped ZnO nanocrystals, which can be easily processed at temperatures much lower than those for the bulk ZnO crystals, are of particular interest because of their potential use in light-emitting devices, when doped with, e.g., rare-earth atoms, or as highly conducting transparent conducting oxides for sensor or solar cell applications. Further, the formation of composites by blending the ZnO nanocrystals and conjugated polymers is attractive for hybrid organic-inorganic photovoltaics because the efficient luminescence from the ZnO counterpart is strongly quenched due to the charge transfer reaction. The expectation is that these blends can allow for the realization of efficient photovoltaic devices with improved stability and conductivity due to the presence of an inorganic counterpart.² The organic-inorganic approach recently demonstrated a high potential of surface capped inorganic semiconducting nanoparticles as the electron acceptor in photovoltaic devices.^{3,4}

Doping ZnO with shallow donors is challenging. The group III elements (Al, Ga, and In) are typical shallow donors in single crystals of ZnO. By using electron paramagnetic resonance (EPR) spectroscopy, the In and Ga shal-

low donors were identified on the basis of the resolved hyperfine (HF) structure in EPR spectra.^{1,5-7} However, since the hyperfine splitting in the EPR signals of Al-doped ZnO single crystals is absent, the identity of Al as the core of the shallow donor has not been unambiguously ascertained so far.

As yet, Al, Ga, and In have not been identified as shallow donors in ZnO nanocrystals. Recently, however, it was demonstrated that interstitial Li and Na atoms form shallow donors in ZnO nanocrystals.⁸⁻¹⁰ The identification was based on the observation of electron-nuclear double resonance (ENDOR) signals of ^7Li (nuclear spin $I=3/2$) and ^{23}Na ($I=3/2$) spins in Li-doped and Na-doped ZnO nanocrystals, respectively. These observations demonstrate the utilizability of the EPR/ENDOR spectroscopy for studying semiconductor nanostructures, especially where the traditional methods of measuring n - and p -type conductivities applicable to bulk semiconductors cannot be used.

The identification of Li and Na as interstitial shallow donors in ZnO nanocrystals is of fundamental interest, but is probably not of great importance for the practical applications in electronic devices where one needs to control the concentration of donor impurities. For this purpose, one should rather dope the nanoparticles with substitutional impurities. In this contribution, we show that ZnO nanocrystals can be doped with Al to form shallow substitutional donors. The identification is provided by the analysis of the EPR signal of this donor and of the ENDOR signals originating from ^{67}Zn and ^{27}Al nuclear spins. It is also shown that a deep Na-related acceptor located at or near the surface of the ZnO nanocrystals is formed and is similar to observations on the Li-doped ZnO nanocrystals.⁸⁻¹⁰

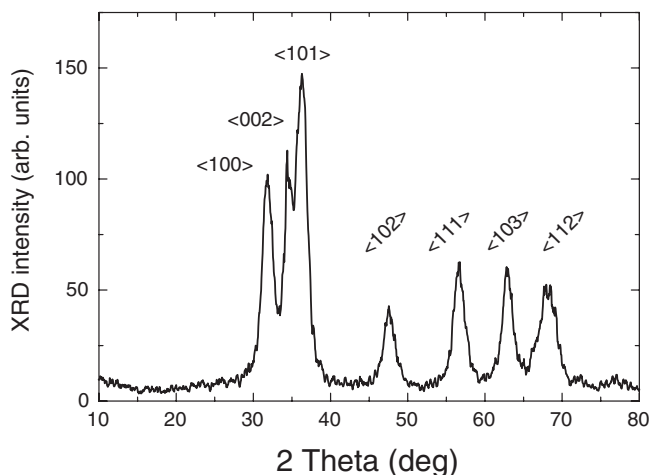


FIG. 1. The XRD powder spectrum of aluminum-doped ZnO nanocrystals.

II. EXPERIMENT

Samples of ZnO doped with Al were prepared in the following way. Some 5 mmol $Zn(Ac)_2 \cdot 2H_2O$ + 0.5 mol % $Al(NO_3)_3 \cdot 9H_2O$ and 7 mmol $LiOH \cdot H_2O$ were separately dissolved in ethanol (50 ml each) and the solutions were subsequently cooled to 0 °C. A lithium hydroxide catalyst was added dropwise to $Zn(Ac)_2 \cdot 2H_2O$ until the solution became transparent. The solution was stored for several hours at 0 °C and was then moved and stored in a refrigerator at 8 °C. ZnO:Al nanoparticles continued to grow, or age, even when stored at 0 °C. It was found that the temperature and the composition of the solution have a marked influence on the rate of particle growth. After a given storage time, a targeted average particle size of the nanoparticles is obtained by precipitation of ZnO:Al by adding an alkane, such as hexane. The supernatant was then removed by repeated decantation or centrifugation (washing). X-ray diffraction (XRD) analysis of the white powder revealed the characteristic wurtzite structure of the ZnO host matrix as shown in Fig. 1. The average particle size was computed by the Scherrer equation to be smaller than 5 nm for the <100> peak.

The EPR and ENDOR experiments were carried out at 1.5–2 K on a home-built 94.9 GHz pulsed EPR/ENDOR spectrometer, which has been described in detail in previous publications.¹¹ ENDOR studies were performed using a pulsed scheme introduced by Mims.¹² Here, a $\pi/2 - \tau - \pi/2 - T - \pi/2$ microwave pulse sequence, applied resonantly with the EPR signal, produces the so-called stimulated echo (SE) signal at time τ after the third $\pi/2$ pulse. Nuclear transitions were induced by a radio-frequency pulse applied between the second and third microwave pulses and monitored as a change of the SE intensity. The ENDOR spectra were recorded via detection of the SE intensity as a function of the radio frequency. The advantage of using high microwave frequency is the high spectral resolution that can be achieved in the EPR as well as in the ENDOR spectra. A very high sensitivity of the pulsed technique as compared to the cw technique facilitated the obser-

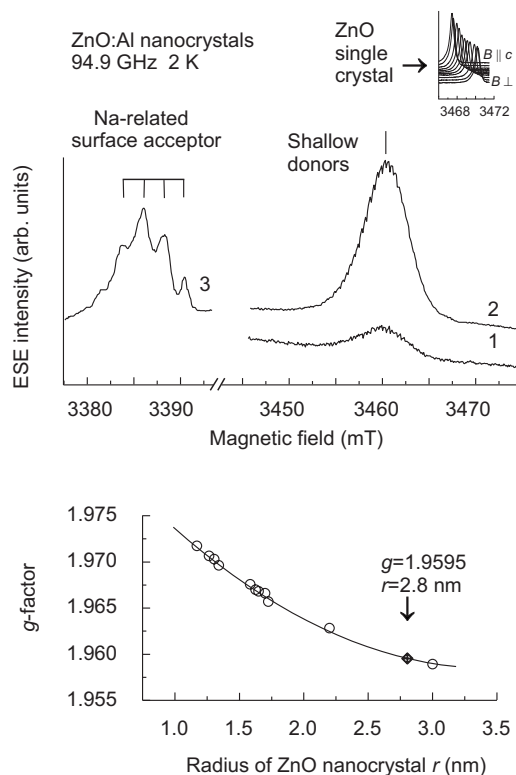


FIG. 2. (Top) The ESE-detected EPR spectrum at 94.9 GHz of the shallow donor in Al-doped ZnO nanoparticles (1) prior and (2) after 30 min UV illumination ($T=2$ K). The EPR line with the four-line hyperfine structure (3) belongs to a Na-related deep acceptor near the surface of ZnO (Ref. 10). (Inset) The ESE spectra of shallow hydrogen donors in ZnO single crystals are shown for several orientations of the magnetic field for comparison. (Bottom) The dependence of the g factor of the shallow donor on the size of ZnO nanocrystals where the diamond indicates the g value of the Al-doped ZnO nanocrystals measured in this work.

vation of ENDOR spectra in this work. A 100 W mercury arc in combination with a water filter was used for the UV illumination.

III. RESULTS AND DISCUSSION

Figure 2 shows the electron spin echo (ESE)-detected EPR spectrum at 94.9 GHz of Al-doped ZnO nanocrystals measured at $T=2$ K. Signals (1) and (2) at the high magnetic field can be assigned to the shallow donors. Signal (1) was obtained without illumination and signal (2) was obtained after 30 min illumination with UV light. The EPR signal (3) at the low magnetic field, with the characteristic four-line hyperfine structure measured after 30 min illumination with UV light, is assigned to a Na-related deep acceptor near the surface of the ZnO nanocrystals.^{8–10}

First, we will concentrate on the EPR signal assigned to the shallow donor. Signals (1) and (2) in Fig. 2 are assigned to a donor because the g factor is smaller than the g value of a free electron. The structureless signal has the linewidth of about 5 mT. Its average g value ($g=1.9595$) differs from the $g_{||}=1.9569$ and $g_{\perp}=1.9552$ values obtained for the shallow

hydrogen donor in a single crystal of ZnO.¹³ However, the difference $g_{\parallel} - g_{\perp} = 0.0017$ partly corresponds to the measured linewidth in ZnO:Al. For comparison, the ESE spectra of the shallow hydrogen donor in a single crystal of ZnO are shown in the inset of Fig. 2 (top) for several orientations of the magnetic field with respect to the c axis. The frequency, the temperature, and the magnetic field scales are the same for ZnO:Al nanocrystals and for ZnO single crystals (inset). If the c axis in a nanocrystal powder was randomly oriented, a linewidth of about 3–4 mT might be expected. This is smaller than the linewidth of the shallow donor signal observed in ZnO:Al nanocrystals. Additional broadening of the ESE line can be due to the size dispersion of about 10% in the ZnO nanocrystals studied.

The average radius of the ZnO:Al nanocrystals was estimated from the observed g value ($g = 1.9595$) to be 2.8 nm. This estimate was obtained by using the dependence of the g value of the EPR signal of the shallow Li donor on the radius of ZnO nanocrystals. In Fig. 2 (bottom), this dependence is shown by the open circles. The diamond indicates the $g = 1.9595$ value observed for the Al-doped nanocrystals. The shift of the g value toward the free-electron value when the size of the nanoparticles decreases is caused by the confinement of the hydrogenlike $1s$ -type wave function of shallow donors when the Bohr radius becomes comparable to the size of the nanoparticles. The effect is explained by the reduction of the admixture of valence-band states and higher-lying conduction bands into the lowest conduction band due to the increase of the band-gap energy and of the energy of higher-lying conduction bands upon the reduction of the size of the nanocrystals.^{8,9,14,15} We believe that the size dependence of the g value of the Li donor can be used to derive the size of the Al-doped nanoparticles because the Bohr radii of the $1s$ wave function of these two donors are almost the same, i.e., about 1.5 nm.

The high magnetic field part of the EPR spectrum ascribed to shallow donors in Fig. 2 does not provide information on the chemical nature of the donor in ZnO:Al since no resolved hyperfine structure is observed, as was, e.g., the case for In and Ga shallow donors in ZnO bulk crystals.¹ To identify the binding core, ENDOR experiments were performed to search for aluminum-related resonances. Indeed, ENDOR signals around the nuclear Zeeman frequency of ^{27}Al nuclei as well as the ENDOR signals corresponding to ^{67}Zn nuclear spins were detected. We were unable to detect any ENDOR transitions in the characteristic frequency ranges of other impurities that could potentially act as a shallow donor.

Figure 3(a) shows the ENDOR signal of the ^{67}Zn nuclei observed in the EPR signal of the ZnO:Al nanocrystals at $B_0 = 3459$ mT. In Fig. 3(a), a broad, unresolved set of ENDOR lines located symmetrically around the Zeeman frequency of ^{67}Zn at 9.24 MHz is seen. This ^{67}Zn ENDOR signal is almost similar to the one observed in the EPR of shallow Li donors in ZnO nanocrystals with a radius of 1.6 nm.^{8,9} This latter spectrum, which is shown as a reference, exhibits a dip in the center that is caused by the nonzero density of the wave function of the shallow donor at the surface of the nanoparticles and the lack of remote ^{67}Zn nuclei. This dip is not visible in the ENDOR spectrum of the

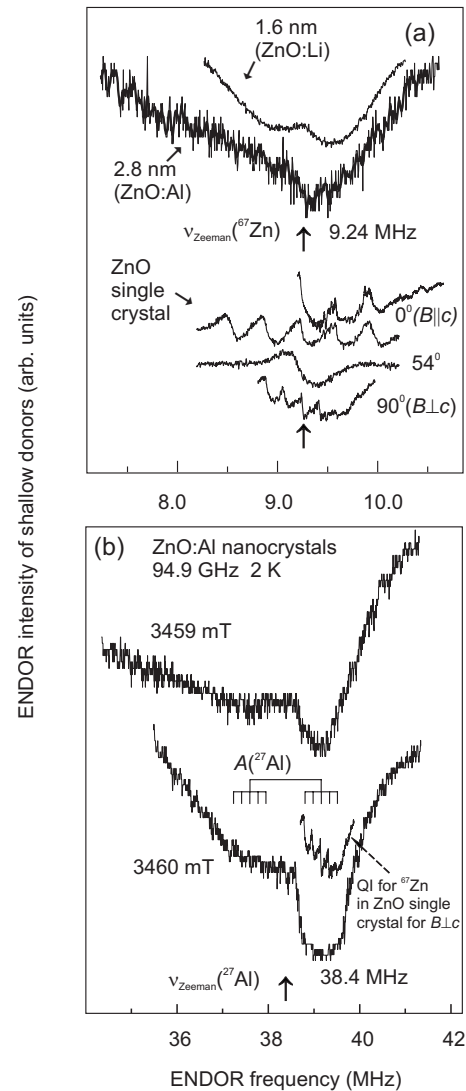


FIG. 3. (a) The ESE-detected ENDOR signal of ^{67}Zn nuclei observed in the EPR signal of the shallow donor in ZnO:Al nanocrystals. The ENDOR spectrum of ^{67}Zn nuclear spins in Li-doped ZnO nanocrystals ($r = 1.6$ nm) is shown for comparison. (Bottom) The ESE-detected ENDOR signals of ^{67}Zn nuclei observed in the EPR signal of the shallow H donor in ZnO single crystals are shown in three orientations [$0^\circ(B\parallel c)$, 54° , and $90^\circ(B\perp c)$]. These three spectra reveal the quadrupole interaction of the ^{67}Zn nuclear spins. The high-frequency part of the ENDOR spectrum with a higher resolution is shown for $B\parallel c$. (b) The ESE-detected ENDOR signal of the ^{27}Al nucleus observed in the EPR signal of the shallow donor in ZnO:Al nanocrystals for two values of the magnetic field: $B_0 = 3459$ mT and $B_0 = 3460$ mT.

Al-doped nanocrystals probably because of the larger size and larger size distribution.

As a reference, the lower part of Fig. 3(a) shows the ENDOR signals of ^{67}Zn nuclei detected via EPR of the H-related shallow donors in ZnO single crystals for three orientations of the magnetic field [$0^\circ(B\parallel c)$, 54° , and $90^\circ(B\perp c)$]. These spectra reveal the quadrupole interaction (QI) with the remote Zn shells. In addition, the high-frequency part of the ENDOR spectrum for $B\parallel c$ measured with higher resolution is blown up to demonstrate that this

spectrum consists of a multitude of ENDOR lines that are related to various Zn shells.

To understand the shape of the ENDOR spectrum related to ^{67}Zn , one should consider the HF interaction between the electron spin of the shallow donor and the nuclear spins, taking the quadrupole interaction of the nuclear spins into account. The isotropic HF interaction a_i reflects the spin density of the shallow donor electron wave function (Ψ) at the nucleus site (r_i): $a_i = (8\pi/3)g_e\beta_e g_n \beta_n |\Psi(r_i)|^2$, where g_e is the electronic g factor, β_e is the electronic Bohr magneton, g_n is the g factor of the ^{67}Zn nucleus, and β_n is the nuclear magneton. The related ENDOR transition frequencies for a paramagnetic center with $S=1/2$ are $\nu_{\text{ENDOR},i} = h^{-1}|g_{ni}\beta_n B_0 \pm a_i/2|$. Thus, each nucleus i gives rise to two ENDOR transitions symmetrically placed around its nuclear Zeeman frequency $g_n\beta_n B_0/h$ when the QI is neglected and when $a_i < g_n\beta_n B_0$. The “+” and “-” signs in the equation denote ENDOR lines for $M_S = +1/2$ and $M_S = -1/2$, respectively. To account for the QI in the case of axial symmetry, an additional term $h^{-1}m_q 3q_i(3\cos^2\Theta - 1)$ should be added to calculate ν_{ENDOR} , where m_q is the average value of the nuclear quantum states $m_I, m_{I'}$, between which the nuclear transition takes place. For axial symmetry, one obtains $q = (eQ_0)/[4I(2I-1)]V_{ZZ}(r_i)$, where Q_0 is the electric quadrupole moment in multiples of $|e| \times 10^{-24}$ cm² and $V_{ZZ}(r_i)$ is the electric-field gradient. For ^{67}Zn nuclei, the nuclear spin $I=5/2$ and $Q_0(^{67}\text{Zn})=0.150$. For $I=5/2$, there are five m_q values: $m_q = \pm 2, \pm 1$, and 0. Thus, the quintet character of the ENDOR spectrum observed in Fig. 3(a) in the EPR spectrum of the shallow donor in the ZnO single crystal is related to QI with remote Zn shells. The angular dependence observed for the quadrupole splitting is typical for the nuclear spin $I=5/2$, with the axially symmetric QI along the c axis. It is remarkable that the ENDOR signals of ^{67}Zn nuclear spins, with their low natural abundance of 4.1%, are so clearly visible. This can be explained by a dynamic nuclear polarization process as observed in Li-doped ZnO nanocrystals.¹⁶

The shape of the ENDOR spectrum of the ^{67}Zn nuclear spins observed in the ZnO nanocrystals is caused by the distribution of quadrupole and HF interactions in the nanocrystal. The broad line is a result of averaging these interactions in the randomly oriented ZnO nanocrystals in contrast to a well resolved structure in single crystals. The dip in the spectrum of the ^{67}Zn nuclei observed for the Li-doped ZnO nanocrystals indicates that for small nanocrystals, the HF interactions with remote Zn shells is missing.

Figure 3(b) shows the ENDOR spectrum of ^{27}Al nuclei as observed in the EPR signal of the shallow donor in ZnO:Al nanocrystals for two values of magnetic field: $B_0=3459$ mT and $B_0=3460$ mT. Two broad ENDOR lines separated symmetrically around the nuclear Zeeman frequency of ^{27}Al ($I=5/2$, abundance 100%) at 38.4 MHz are seen. This splitting is due to the HF interaction with ^{27}Al and corresponds to the HF interaction constant $A(^{27}\text{Al})=1.45$ MHz. For $B_0=3460$ mT, a boxlike distribution of ENDOR lines is observed. It is rather surprising that the small shift in the magnetic field of 1 mT leads to a marked difference in the shape of the ^{27}Al ENDOR spectrum

displayed in Fig. 3(b). Since there is a substantial contribution of g anisotropy to the linewidth of the EPR line, we think that the difference in shape is partly caused by the orientation selectivity and this field mainly selects a set of nanocrystals with their c axis perpendicular to the magnetic field. The boxlike form of the ENDOR spectrum is caused by the quadrupole splitting that gives rise to five unresolved lines of the ^{27}Al nuclei with a quadrupole moment $Q_0(^{27}\text{Al})=0.150$. It is important to note that the value of the QI of ^{27}Al is nearly the same as the QI for ^{67}Zn nuclear spins in ZnO. Moreover, the nuclear spins and the quadrupole moments of ^{27}Al and ^{67}Zn are the same, too. As a reference, the ENDOR spectrum of the ^{67}Zn nuclei, detected via EPR of the shallow H donor in ZnO single crystals with $B \perp c$, is shown on the same scale as the ENDOR signals of ^{27}Al in Fig. 3(b). This indicates that the intrinsic electric-field gradients at the Zn nuclear sites and Al site seem to be virtually the same. This finding is taken to support the assumption that Al enters the ZnO nanocrystals substitutionally and that it is centrally located at the Zn site. Consequently, it may form a core for the shallow donor electron in the ZnO:Al nanocrystals. This is not obvious because the smaller radius of Al^{3+} (0.51 Å compared to 0.74 Å for Zn^{2+}) could drive the impurity into the off-center position.

For a quantitative analysis of the observed isotropic HF constants for an Al-related shallow donor, the expression given above indicates that it is necessary to determine the spin density $|\Psi(r_i)|^2$ at the Al nucleus. Our analysis is based on the prediction of effective mass theory, in which the ground state of a shallow donor in semiconductors can be described by a hydrogenlike $1s$ wave function $\Phi(r) \sim \exp(-r/r_D)$,^{16,17} where r_D is the effective Bohr radius of the shallow donor. The simplest description of the energy levels of a shallow electron center resembles that of atomic hydrogen, with an electron of effective mass m^* in a medium of dielectric constant ϵ . The scaled radius of the lowest $1s$ -like energy state is given by $r_D = (r_H R_H)/(E_D \epsilon)$, where E_D is the binding energy, r_H is the Bohr radius (0.0529 nm), and R_H represents the Rydberg constant (13.6 eV). By using this equation, we can calculate the shallow donor radius r_D based on experimental values of the binding energies E_D . The binding energy E_D for substitutional Al, Ga, and In donors are 51.55, 54.6, and 63.2 meV, respectively.¹ The Bohr radii for Al, Ga, and In shallow donors are found to be 1.93, 1.73, and 1.63 nm, respectively.

It has been shown in Refs. 18 and 19 that, by orthogonalizing a suitable envelope function $\Phi(r)$ to the cores of the lattice ions to satisfy the Pauli principle, the spin density on nucleus i can be written as an amplification factor K_i times the density of the envelope function Φ at nucleus i . If the envelope function remains nearly the same within each ion core (which is the case for a strongly delocalized envelope function Φ), the value of K_i will only depend on the species of ion i and not on its position in the lattice. Thus, $|\Psi(r_i)|^2 = K_i |\Phi(r_i)|^2$. We can then rewrite the equation for the isotropic HF interaction constant for the shallow donor (SD) as $A(\text{SD}) = (8\pi/3)g_e\beta_e g_n \beta_n K_{\text{SD}} |\Phi(r_i)|^2$, where K_{SD} is the amplification factor for the Al, Ga, and In shallow donors, respectively. If we place the Al (Ga, In) nuclei at the

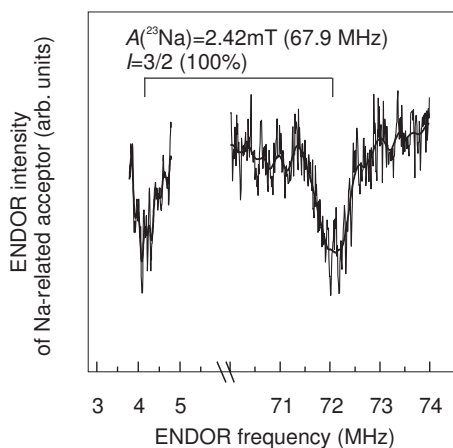


FIG. 4. The ESE-detected ENDOR signals of ^{23}Na nuclei as observed in the EPR signal of a deep Na-related acceptor center in Al-doped ZnO nanocrystals. The sample was illuminated for 30 min with UV light before the EPR and ENDOR were recorded ($\nu = 94.9$ GHz, $T=2$ K).

Coulomb center of the shallow donor, we can estimate the densities of the envelope function Φ at the center: $|\Phi_{\text{Al}}(0)|^2 = 0.910 \times 10^{-5}$ a.e., $|\Phi_{\text{Ga}}(0)|^2 = 1.09 \times 10^{-5}$ a.e., and $|\Phi_{\text{In}}(0)|^2 = 1.68 \times 10^{-5}$ a.e.

The experimental HF interaction constant of the shallow In donors was found to be $A(^{115}\text{In}) = 36.6$ G = 100.3 MHz,^{5,6} and that for the shallow Ga donor to be $A(^{69}\text{Ga}) = 4.2$ G = 11.5 MHz (Ref. 5) or $A(^{69}\text{Ga}, ^{71}\text{Ga}) = 6.7$ G = 18.4 MHz.⁷ We will use the average values $A(^{69}\text{Ga}) = 6$ G = 16.8 MHz and $A(^{27}\text{Al}) = 1.45$ MHz (this work). To compare these values, one should scale the HF interactions by the corresponding nuclear g value. The experimental values obtained in this way are $|\Psi_{\text{Al}}(0)|^2 = 0.00124$ a.e., $|\Psi_{\text{Ga}}(0)|^2 = 0.0153$ a.e., and $|\Psi_{\text{In}}(0)|^2 = 0.102$ a.e. The amplification factors K for Al, Ga, and In are $K_{\text{Al}} = 137$, $K_{\text{Ga}} = 1433$, and $K_{\text{In}} = 6070$, obtained by using the experimental values of $|\Psi(0)|^2$. For the calculation of K , we used $|\Phi(0)|^2$ values; thus, the K values are only partly based on experimental findings.

The quartet character of the EPR signal (3) in Fig. 2 indicates a nearly isotropic HF interaction with a nucleus having spin $I=3/2$ and an almost 100% abundance. This observation favors a Na-related center (^{23}Na , $I=3/2$, 100%) and, indeed, the ENDOR study of this signal reveals two transitions at 4.2 and 72.0 MHz as shown in Fig. 4. According to the equation for ν_{ENDOR} given above, one can find the hyperfine constant for ^{23}Na of $A=67.9$ MHz, which corresponds to the HF splitting of 2.42 mT observed in the EPR line shape.

In the study of Li-doped ZnO nanoparticles, an EPR signal with quartet structure similar to the one shown in Fig. 2 and a related ENDOR signal similar to that displayed in Fig. 4 were observed.^{8,9} In this earlier study, it was concluded that

the deep Na-related center is located close to or at the ZnO/Zn(OH)₂ interface, because not only the ENDOR signals of the ^{23}Na ($I=3/2$) nucleus, but also the ENDOR signal of ^1H ($I=1/2$) nuclear spins of the Zn(OH)₂ capping layer could be observed. This latter observation demonstrates that the density of the localized electronic wave function of the Na-related acceptor is relatively large in the Zn(OH)₂ capping layer. The ENDOR signal of ^1H was not observed in the Al-doped ZnO:Al nanocrystals since there was no Zn(OH)₂ capping layer. From the similarity of the g values, the HF structure of the EPR line shapes, and the position of the observed ENDOR signals, we conclude that the Na-related deep acceptor is also located close to or at the surface of the nanoparticles in ZnO:Al studied here. Following Fig. 2, the paramagnetic state of a Na-related acceptor is formed under UV illumination along with the Al-related shallow donor.

IV. CONCLUSION

The EPR and ENDOR studies at 95 GHz unambiguously show that Al can be substitutionally introduced in the ZnO nanocrystal to form shallow effective-masslike donors. The Al is positioned at the center of a Zn position as shown by the intrinsic electric-field gradients at the Al nucleus, which are the same as those at the Zn nucleus. The shallow character of the Al donor is evidenced by the multitude of ^{67}Zn ENDOR lines and, further, by the hyperfine interactions with the ^{27}Al nucleus of 1.45 MHz, which is much weaker than for atomic aluminum. The radius of ZnO nanocrystals containing the shallow Al donor was deduced to be 2.8 nm from the g -factor value. The most probable position of the substitutional Al shallow donor with its large Bohr radius is near the center of a ZnO nanocrystal. The detailed understanding of the doping mechanism of ZnO nanocrystals on a microscopic level is important for the application of these transparent, highly conducting, and easily processable nanocrystalline systems for optoelectronics and photovoltaics.

ACKNOWLEDGMENTS

This work forms part of the research program of the Netherlands Foundation for Fundamental Research of Matter (F.O.M.) and the Technology Foundation STW, with financial support from the Nederlandse Organisatie voor Wetenschappelijk Onderzoek (N.W.O.). Financial support from the SENTINEL Network in the framework of the 5th EC Science Program is acknowledged. The support of the Russian Foundation for Basic Research, the programs under the Russian Academy of Sciences “Spintronics,” P-03, and “Quantum Macrophysics,” and the St. Petersburg Scientific Center is gratefully acknowledged. I.R., D.R., V.L., and V.D. also acknowledge the financial support by the Bavarian Ministry of Economic Affairs, Infrastructure, Transport and Technology (BayStMWIVT).

- *Also at Federal Center of Shared Facilities of Kazan State University, 42008 Kazan, Russia.
†pavel.baranov@mail.ioffe.ru
‡Also at Bavarian Centre for Applied Energy Research (ZAE Bayern), Am Hubland, 97074 Würzburg, Germany; dyakonov@physik.uni-wuerzburg.de
- ¹B. K. Meyer, H. Alves, D. M. Hofmann, W. Kriegseis, D. Forster, F. Bertram, J. Christen, A. Hoffmann, M. Straßburg, M. Dworzak, U. Haboeck, and A. V. Rodina, *Phys. Status Solidi B* **241**, 231 (2004).
 - ²W. J. E. Beek, M. M. Wienk, and R. A. J. Janssen, *Adv. Funct. Mater.* **16**, 1112 (2006).
 - ³M. Pientka, V. Dyakonov, D. Meissner, A. Rogach, D. Talapin, H. Weller, L. Lutsen, and D. Vanderzande, *Nanotechnology* **15**, 163 (2004).
 - ⁴W. U. Huynh, J. J. Dittmer, and A. P. Alivisatos, *Science* **295**, 2425 (2002).
 - ⁵C. Gonzalez, D. Block, R. T. Cox, and A. Hervé, *J. Cryst. Growth* **59**, 357 (1982).
 - ⁶D. Block, A. Hervé, and R. T. Cox, *Phys. Rev. B* **25**, 6049 (1982).
 - ⁷N. Y. Garces, N. C. Giles, L. E. Halliburton, G. Cantwell, D. B. Eason, D. C. Reynolds, and D. C. Look, *Appl. Phys. Lett.* **80**, 1334 (2002).
 - ⁸S. B. Orlinskii, J. Schmidt, P. G. Baranov, D. M. Hofmann, C. de Mello Donegá, and A. Meijerink, *Phys. Rev. Lett.* **92**, 047603 (2004).
 - ⁹S. B. Orlinskii, J. Schmidt, E. J. J. Groenen, P. G. Baranov, C. de Mello Donegá, and A. Meijerink, *Phys. Rev. Lett.* **94**, 097602 (2005).
 - ¹⁰S. B. Orlinskii, H. Blok, J. Schmidt, P. G. Baranov, C. de Mello Donegá, and A. Meijerink, *Phys. Rev. B* **74**, 045204 (2006).
 - ¹¹J. A. J. M. Disselhorst, H. Vandermeer, O. G. Poluektov, and J. Schmidt, *J. Magn. Reson., Ser. A* **115**, 183 (1995).
 - ¹²W. B. Mims, in *Electron Paramagnetic Resonance*, edited by S. Geschwind (Plenum, New York, 1972).
 - ¹³D. M. Hofmann, A. Hofstaetter, F. Leiter, H. Zhou, F. Henecker, B. K. Meyer, S. B. Orlinskii, J. Schmidt, and P. G. Baranov, *Phys. Rev. Lett.* **88**, 045504 (2002).
 - ¹⁴D. M. Hofmann, H. Zhou, D. R. Pfisterer, H. Alves, B. K. Meyer, P. Baranov, N. Romanov, C. de Mello Donegá, A. Meijerink, S. Orlinskii, H. Blok, and J. Schmidt, *Phys. Status Solidi C* **1**, 908 (2004).
 - ¹⁵A. V. Rodina, L. Efros, M. Rosen, and B. K. Meyer, *Mater. Sci. Eng., C* **19**, 435 (2002).
 - ¹⁶K. W. Boer, *Survey of Semiconductor Physics* (Van Nostrand Reinhold, New York, 1990).
 - ¹⁷A. M. Stoneham, *Theory of Defects in Solids* (Clarendon, Oxford, 1985).
 - ¹⁸B. S. Gourary and F. S. Adrian, *Solid State Phys.* **10**, 127 (1960).
 - ¹⁹M. T. Bennebroek, A. Arnold, O. G. Poluektov, P. G. Baranov, and J. Schmidt, *Phys. Rev. B* **54**, 11276 (1996), and references therein.